

Modulating Charge Separation Efficiency of Water Oxidation Photoanodes with Polyelectrolyte-Assembled Interfacial Dipole Layers

Sanghyun Bae, Dongseok Kim, Hyunwoo Kim, Minsu Gu, Jungki Ryu,*
and Byeong-Su Kim*


The charge separation efficiency of water oxidation photoanodes is modulated by depositing polyelectrolyte multilayers on their surface using layer-by-layer (LbL) assembly. The deposition of the polyelectrolyte multilayers of cationic poly(diallyldimethylammonium chloride) and anionic poly(styrene sulfonate) induces the formation of interfacial dipole layers on the surface of Fe_2O_3 and TiO_2 photoanodes. The charge separation efficiency is modulated by tuning their magnitude and direction, which in turn can be achieved by controlling the number of bilayers and type of terminal polyelectrolytes, respectively. Specifically, the multilayers terminated with anionic poly(styrene sulfonate) exhibit a higher charge separation efficiency than those with cationic counterparts. Furthermore, the deposition of water oxidation molecular catalysts on top of interfacial dipole layers enables more efficient photoelectrochemical water oxidation. The approach exploiting the polyelectrolyte multilayers for improving the charge separation efficiency is effective regardless of pH and types of photoelectrodes. Considering the versatility of the LbL assembly, it is anticipated that this study will provide insights for the design and fabrication of efficient photoelectrodes.

1. Introduction

Solar production of chemicals is a potential route for storing and utilizing unlimited, albeit intermittent, solar energy.^[1–6] In principle, all types of semiconductors with a proper bandgap can absorb sunlight, generate excitons, and drive electrochemical reactions to produce valuable chemicals such as hydrogen^[2]

S. Bae, H. Kim, Prof. J. Ryu
Department of Energy Engineering
School of Energy and Chemical Engineering
Emergent Hydrogen Technology R&D Center
Ulsan National Institute of Science and Technology (UNIST)
Ulsan 44919, Republic of Korea
E-mail: jryu@unist.ac.kr

D. Kim, Dr. M. Gu, Prof. B.-S. Kim
Department of Chemistry
Yonsei University
Seoul 03722, Republic of Korea
E-mail: bskim19@yonsei.ac.kr

 The ORCID identification number(s) for the author(s) of this article can be found under <https://doi.org/10.1002/adfm.201908492>.

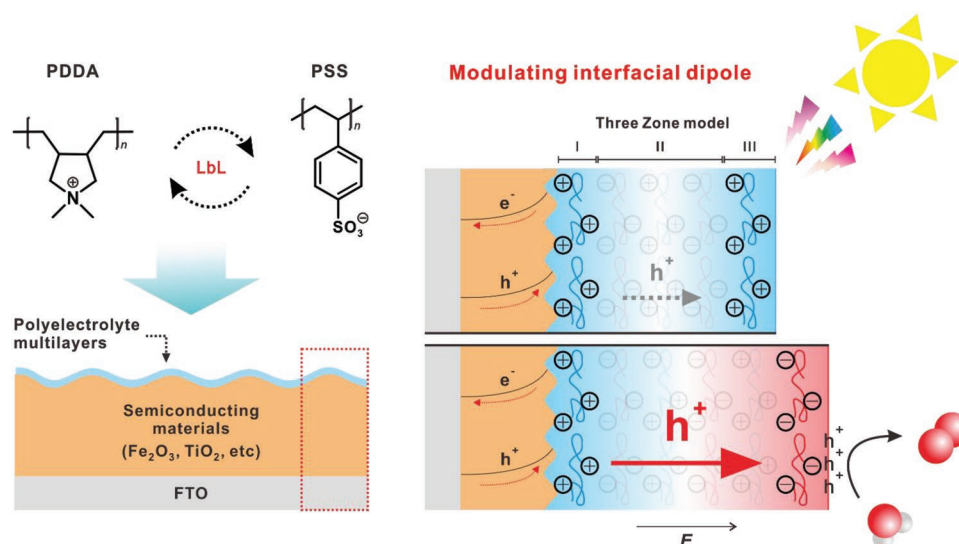
DOI: 10.1002/adfm.201908492

and hydrocarbons.^[4] In this regard, various materials are being explored for efficient photogeneration of excitons and their catalytic applications, including Fe_2O_3 ,^[7–9] BiVO_4 ,^[10–12] WO_3 ,^[13–15] and TiO_2 ,^[16,17] as water oxidation photoanodes; Si ,^[18,19] and Cu_2O ^[20,21] as water reduction photocathodes; and cobalt phosphate^[11,22] and Pt nanoparticles^[23,24] as redox catalysts. However, most semiconductors retain inherent problems such as the short diffusion length of charge carriers,^[25] high recombination rate,^[26] and low charge separation efficiency.^[27] These, in turn, result in low overall performance. In this aspect, charge separation efficiency is regarded as the most critical factor for improving the performance of photoelectrodes.

In order to improve the charge separation efficiency, various strategies have been suggested to date, such as nanofabrication of photoelectrodes, formation of heterojunction,^[28–30] defect engineering,^[31]

and introduction of surface dipoles.^[32] In general, the migration of charge carriers in bulk electrodes and their recombination at the photoelectrode–electrolyte interface are considered two major factors determining the charge separation efficiency of the photoelectrodes.^[33] In particular, it was reported that the separation efficiency can be improved by controlling at least one dimension of photoelectrodes shorter than the diffusion length of the charge carriers^[34] or by introducing a heterojunction structure for band engineering.^[28,30] However, these approaches address only the charge migration issue, while raising other problems. For example, they can result in the formation of extensive interfacial defects, which exacerbate the recombination and stability issues.^[35,36] In this regard, it is necessary to develop a complementary approach that can address the aforementioned issues comprehensively.

In this study, we report the improvement in the charge separation efficiency of photoelectrodes with polyelectrolyte multilayers. Cationic and anionic polyelectrolytes can be readily assembled using electrostatic interactions by exploiting a versatile layer-by-layer (LbL) assembly to form multilayers with interfacial dipole moments. Their magnitude and direction can be fine tuned by controlling the number of bilayers (BL)



Scheme 1. Schematic illustrations of LbL assembled polyelectrolyte multilayers on photoelectrode and simplified carrier pathway for enhanced charge-separation toward efficient water oxidation. The LbL multilayer is drawn not to the scale.

of oppositely charged polyelectrolytes and the type of terminal polyelectrolyte in the multilayers. As a model photoanode, Fe_2O_3 and TiO_2 are modified with multilayers of strong polyelectrolytes—cationic poly(diallyldimethyl ammonium chloride) (PDDA) and anionic poly(styrene sulfonate) (PSS). Photoelectrochemical (PEC) characterizations combined with electrochemical impedance spectroscopy (EIS) and Mott–Schottky analysis demonstrate that the charge separation efficiency can be modulated by the dipole moments of the polyelectrolyte multilayers, independent of the pH and types of photoanodes tested. In general, photoanodes coated with the polyelectrolyte multilayers terminated with PSS exhibit a higher efficiency than those with PDDA. Furthermore, the deposition of molecular catalysts on top of interfacial dipole layers enables more efficient PEC water oxidation. Considering the substrate- and pH-independent versatility of this LbL approach, we anticipate that this study can enable the design and fabrication of diverse and efficient photoelectrodes.

2. Results and Discussion

The modulation of the charge separation efficiency of photoelectrodes with polyelectrolyte-assembled interfacial dipole layers is schematically depicted in **Scheme 1**. LbL assembly is particularly well suited for formation of interfacial dipole layers, as it enables the assembly of polyelectrolyte multilayers at a nanometer-scale precision regardless of electrode structures without altering the bulk properties of photoelectrodes.^[37,38] Thus, the bulk properties of photoelectrodes, such as bandgap and conductivity, remain intact while their interfacial properties could be engineered. In this study, PDDA and PSS were selected as the cationic and anionic polyelectrolytes for modifying photoanodes, owing to the following characteristics: i) high electrochemical stability (Figure S1, Supporting Information), ii) distinct charge density independent of external pH as strong electrolytes, and thereby, and iii) formation of stable

polyelectrolyte multilayers on various photoanodes, which have different stability and/or operating pH windows. Hereafter, the polyelectrolyte multilayers with negative terminal charge (i.e., PSS as a terminal layer) are denoted by integers, and those with positive terminal charge (i.e., PDDA) by decimal numbers. For example, 3 BL represents polyelectrolyte multilayers composed of three alternating layers of PDDA and PSS on the photoanode, whereas 3.5 BL represents multilayers composed of 3 BL with an additional PDDA layer.

The structure and properties of the LbL-assembled polyelectrolyte multilayers can be explained by the three Zone model:^[39,40] Zone I is denoted as the first polyelectrolyte layer interfacing with the underlying substrate, Zone II as an intermediate charge-compensation region with free mobile ions, and Zone III as the outermost layer. An important feature of the polyelectrolyte multilayers is that their overall thickness and the type of polyelectrolytes in Zone III could be controlled precisely, thereby enabling precise manipulation of the direction and magnitude of the interfacial dipole moment. In this regard, we anticipated that the charge separation efficiency near the photoelectrode–electrolyte interface can be tuned by manipulating the properties of the polyelectrolyte multilayers.

Initially, the successful assembly of polyelectrolyte multilayers was investigated using Fe_2O_3 as a model photoanode substrate because of its prominent advantages (e.g., relatively small bandgap and abundance) and disadvantages (e.g., low charge separation efficiency and catalytic activity for water oxidation). Transmission electron microscopy (TEM), combined with energy-dispersive X-ray spectroscopy (EDS), revealed the uniform and conformal deposition of polyelectrolyte multilayers on the surface of worm-like Fe_2O_3 photoanodes (**Figure 1a** and **Figure S2**, Supporting Information). According to EDS elemental mapping analysis, the S that originated from the PSS was distributed uniformly along the coating layers on the Fe_2O_3 photoanode. It should be noted that the contrast difference in the polyelectrolyte multilayers originated from the Pt sputtering

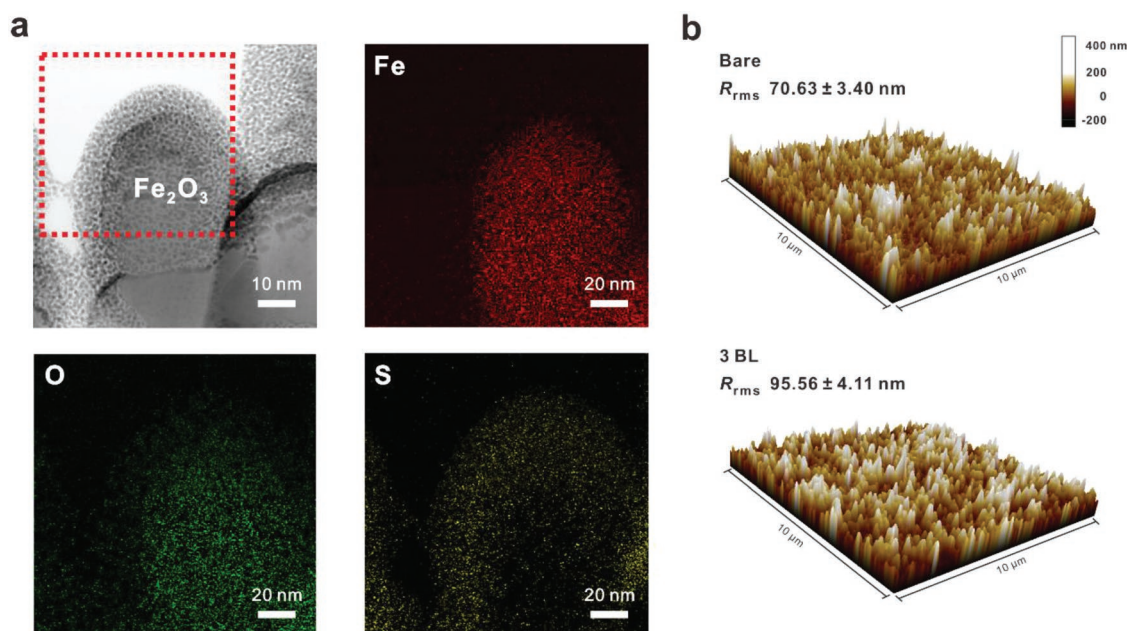


Figure 1. Characterization of polyelectrolyte multilayers assembled on Fe_2O_3 electrode. a) TEM and the corresponding EDS elemental mapping images of 3 BL. b) AFM surface morphology of bare Fe_2O_3 and 3 BL with R_{rms} values averaged over $10 \times 10 \mu\text{m}^2$.

layer that resulted from the preparation of samples for cross-sectional analysis using focused-ion beam etching.

The uniform deposition of the multilayers was further verified by UV/vis spectroscopy and ellipsometry using quartz slide and silicon wafer as a substrate, respectively (Figure S3, Supporting Information). The average thickness of each BL was determined to be 1.87 ± 0.48 nm. The successive deposition of each polyelectrolyte was also investigated by X-ray photoelectron spectroscopy. While the Fe 2p and Sn 3d peaks from the underlying Sn-doped Fe_2O_3 electrode decreased with the number of BL, the N 1s and S 2p peaks increased originated from PDDA and PSS, respectively (Figure S4, Supporting Information). In addition, atomic force microscopy (AFM) confirmed that the assembled polyelectrolyte multilayers became distributed over the entire film surface with the successful growth of polyelectrolyte multilayers on the Fe_2O_3 . The root-mean-square roughness (R_{rms}) increased gradually from 70.63 ± 3.40 nm for the bare Fe_2O_3 to 95.56 ± 4.11 nm for 3 BL, and then decreased to 78.41 ± 6.87 nm for 5 BL of the assembled (PDDA/PSS) multilayer (Figure 1b and Figure S5, Supporting Information). This result indicates that the non-uniform surface of the bare Fe_2O_3 was propagated further with assembled polyelectrolyte multilayers in the lower number of layers (<3 BL). However, with an increased number of layers, the polyelectrolytes multilayers yielded a homogeneous morphology by offsetting the surface roughness of bare Fe_2O_3 . These results evidently demonstrate the uniform and conformal deposition of PDDA and PSS on the surface of the Fe_2O_3 photoanode by the LbL method.

We then investigated the effect of the interfacial polyelectrolyte multilayers on the PEC performance of the Fe_2O_3 photoanodes. Linear sweep voltammetry (LSV) was performed in 80×10^{-3} M potassium phosphate buffer (pH 8.0) under visible light irradiation. First, we examined the effect of the thickness of the polyelectrolyte multilayers (i.e., BL) (Figure 2a and

Figure S6, Supporting Information). While depositions of 1 and 5 BLs had negligible effects, it was noteworthy that the deposition of 3 BLs resulted in a cathodic shift of the onset potential from 0.98 to 0.94 V versus reversible hydrogen electrode (RHE). This was accompanied by a considerable increase in the photocurrent density from 0.32 to 0.41 mA cm^{-2} at 1.6 V versus RHE even without water oxidation catalysts. To further investigate the effect of the interfacial dipole layer, the polyelectrolyte multilayers were assembled under different ionic strengths. We observed that the photocurrent density decreased remarkably when NaCl was added in the polyelectrolyte solutions during the LbL assembly process. This is owing to the charge screening effect of counterions, which reduced the interfacial dipole force of the polyelectrolyte multilayers (Figure S7, Supporting Information).

Independent from the above observation, the Mott–Schottky analysis revealed that the deposition of the polyelectrolyte multilayers resulted in an anodic shift in the flat-band potential of Fe_2O_3 (inset in Figure 2a). This is possibly due to the formation of a dipole moment, which can facilitate the charge separation near the photoelectrode–electrolyte interface.^[41] Similar to the trend in the PEC performance, the 3 BL polyelectrolyte multilayer-modified Fe_2O_3 exhibited the largest shift in the flat-band potential (from 0.25 to 0.49 V versus RHE), implying the generation of the highest dipole moment. Further deposition of the polyelectrolyte multilayers may lead to a longer separation of positively and negatively charged initial and terminal layers (i.e., Zones I and III), thereby diminishing the magnitude of the dipole moment. To exclude the possibility that the improved performance had originated from the increase in surface area,^[42,43] the electric double layer capacitance (C_{dl})—which is proportional to the electrochemically active surface area—of the Fe_2O_3 photoanodes was measured. The double layer capacitance of Fe_2O_3 was marginally decreased from 19.7 to 17.6 $\mu\text{F cm}^{-2}$

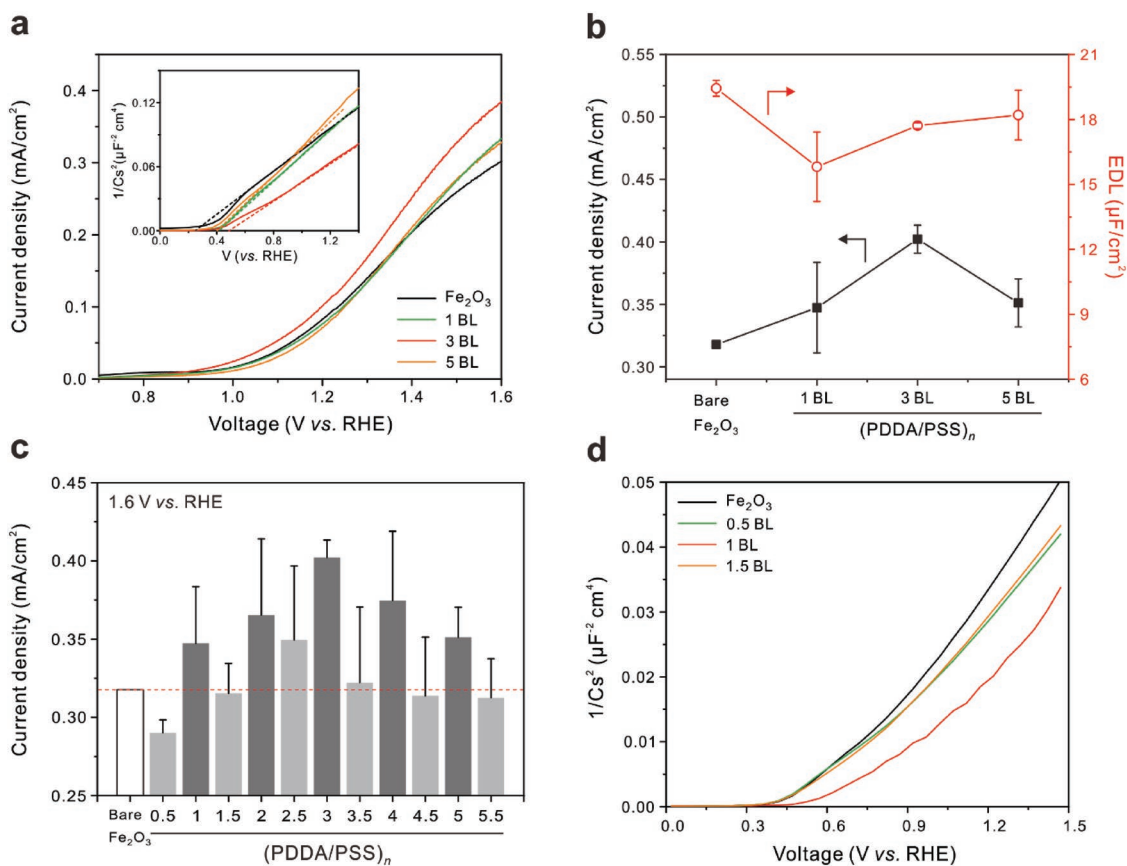


Figure 2. PEC characterizations of Fe_2O_3 photoanodes modified with polyelectrolyte multilayers. a) Representative LSV and a, inset) Mott-Schottky analysis of Fe_2O_3 photoanode assembled with polyelectrolyte multilayers (1, 3, and 5 BL). b) Effect of number of BLs on photoelectrochemical performance (in terms of current density at 1.6 V versus RHE) and specific surface area (in terms of electrical double layer capacitance) of Fe_2O_3 photoanodes. c) Effect of number of BL and types of terminal polyelectrolytes on performance of Fe_2O_3 photoanodes. Note the PDDA terminal layer in gray and PSS in dark gray. d) Mott-Schottky analysis of corresponding photoanodes with polyelectrolyte multilayers.

after the deposition of $(\text{PDDA}/\text{PSS})_n$ polyelectrolyte multilayers for 3 BL (Figure 2b and Figure S8, Supporting Information). The decrease in capacitance can be attributed to the deposition of electrochemically inactive polyelectrolytes and implies the more favorable effect of polyelectrolyte multilayers in improving the performance of photoelectrodes.

Furthermore, we studied the effect of the type of terminal layers on the PEC performance of Fe_2O_3 photoanodes. Most notably, the performance of the Fe_2O_3 photoanodes varied in an alternating manner (Figure 2c). Specifically, Fe_2O_3 with polyelectrolyte multilayers terminated with anionic PSS exhibited a higher photocurrent density than those with a cationic PDDA terminal layer. To elucidate the mechanism underlying this observation, we measured the flat-band potential of Fe_2O_3 photoanodes upon deposition of 0.5, 1.0, and 1.5 BLs (Figure 2d). Both the PEC performance and flat-band potential of the Fe_2O_3 photoanode exhibited a similar trend of variation. Whereas the variations for 0.5 and 1.5 BLs were negligible, the deposition of 1.0 BL resulted in both a performance improvement (in terms of onset potential and photocurrent density) and an anodic shift in the flat-band potential. These results suggest that the modulation of the PEC performance resulted from interfacial dipole layers. Their direction and magnitude can be precisely

controlled with the number of BL in the polyelectrolyte multilayers. It is noteworthy that the Mott-Schottky curves of the Fe_2O_3 photoanode became more linear after the deposition of the polyelectrolyte multilayers. According to the literature, this can be ascribed to the improved band pinning of photoelectrodes by surface-state passivation.^[44,45] It can facilitate efficient charge separation for the water oxidation reaction.

To understand how the interfacial dipole moment created by the polyelectrolyte multilayers can modulate the PEC performance of an underlying photoanode, we performed EIS. The measured EIS spectra were well fitted and analyzed using a 2-RC equivalent circuit (Figure 3a, b and Figure S9a, Supporting Information). The suggested equivalent circuit is composed of the space-charge capacitance (C_{SC}) of the bulk Fe_2O_3 , carrier migration resistance (R_{BULK}) from the bulk Fe_2O_3 to the surface, surface-state capacitance (C_{SS}) associated with charge separation, and charge transfer resistance (R_{CT}) by the electrochemical reactions at the photoelectrode-electrolyte interface.^[12] As expected, there were negligible variations in the bulk properties of the Fe_2O_3 photoanode, such as R_{bulk} and C_{SC} , after the deposition of 3 BLs (data not shown). In contrast, there was a significant variation in interfacial properties such as C_{SS} (Figure 3c) and R_{CT} (Figure 3d). For example, the 3 BL displayed a higher

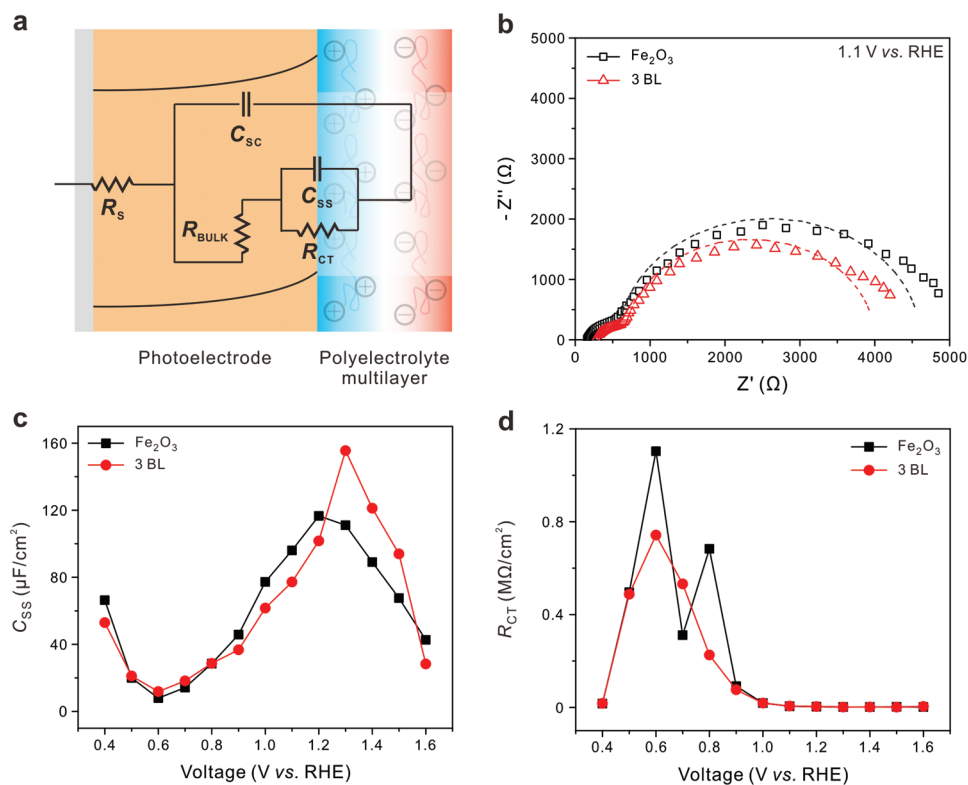


Figure 3. a) Schematic illustration of kinetic analysis for improved PEC water oxidation of photoanode fabricated with polyelectrolyte multilayer. b) Nyquist plot for kinetic analysis of bare Fe_2O_3 and 3 BL. c,d) EIS analysis for elucidating the mechanism of improvement in PEC performance by the fitting of Nyquist plot. c) C_{SS} , and d) R_{CT} .

C_{SS} and a lower R_{CT} than the pristine one. According to the literature, the improved C_{SS} and R_{CT} values can be a measure of the photoelectrode performance; the increase in C_{SS} can be caused by the efficient separation and accumulation of charge carriers and the decrease in R_{CT} by reduced surface recombination.^[44–46] The charge separation efficiency was quantitatively compared in terms of the shift in the flat-band potential before and after light irradiation (ΔV_{FB}) and charging of the surface state ($\Delta V_{charging}$). The 3 BL displayed 1.2-fold higher ΔV_{FB} (205 versus 173 mV) and $\Delta V_{charging}$ (4.06 versus 3.41 V) than the pristine one (Table 1 and Figure S9b, Supporting Information). According to the literatures, ΔV_{FB} and $\Delta V_{charging}$ are proportional to the charge separation efficiency^[44] and the amount of accumulated charge carriers,^[45] respectively.

Taken together, our analyses suggest that the deposition of polyelectrolyte multilayers can improve the charge separation efficiency of Fe_2O_3 photoanodes by forming an interfacial dipole moment (Figure 4a). The interfacial dipole layers may

Table 1. Flat-band potential shift (ΔV_{FB}) between dark and light condition and evaluation of charging of surface state ($\Delta V_{charging}$) in Fe_2O_3 photoanodes. $\Delta V_{charging}$ was estimated by dividing the total charge of C_{SS} by the EDL value (C_{dl}).

Photoanode	ΔV_{FB} [mV]	Q_{tot} [C cm^{-2}]	C_{dl} [F cm^{-2}]	$\Delta V_{charging}$ [V]
Bare Fe_2O_3	173	6.72×10^{-5}	1.97×10^{-5}	3.41
3 BL	205	7.15×10^{-5}	1.76×10^{-5}	4.06

induce upward bending of the vacuum energy level near the photoelectrode–electrolyte interface, thereby providing a higher thermodynamic driving force for efficient separation of charge carriers.

We also measured the LSV curves in the absence and presence of sacrificial electron donor (1 M Na_2SO_3) to decouple the effect of the interfacial dipole layers and the slow water oxidation kinetics on the charge separation efficiency (Figure 4b and Figure S10, Supporting Information). It is noteworthy here that the surface modification of photoanodes for enhanced PEC performance generally results in a decrease in the PEC performance with respect to the oxidation of sacrificial electron donors.^[47] This is because surface recombination rather than oxidation reactions becomes the rate-determining step in the presence of sacrificial donors.^[8] However, the number of interfacial recombination sites can be increased after the modification with polyelectrolyte multilayers assembled on top. Unlike these results, the modification of Fe_2O_3 photoanodes with 3 BL of (PDDA/PSS) improved the PEC performance even with respect to the oxidation of sacrificial donors. We consider that the discrepancy was caused by the different mechanisms for improving the charge separation efficiency. While most conventional materials such as cobalt phosphate can improve the separation efficiency by self-redox reactions,^[11,22] the polyelectrolyte-based dipole layers can improve the efficiency by providing a potential gradient as observed in this study.

To demonstrate the practical application of the polyelectrolyte-based dipole layers, Fe_2O_3 photoanodes were further

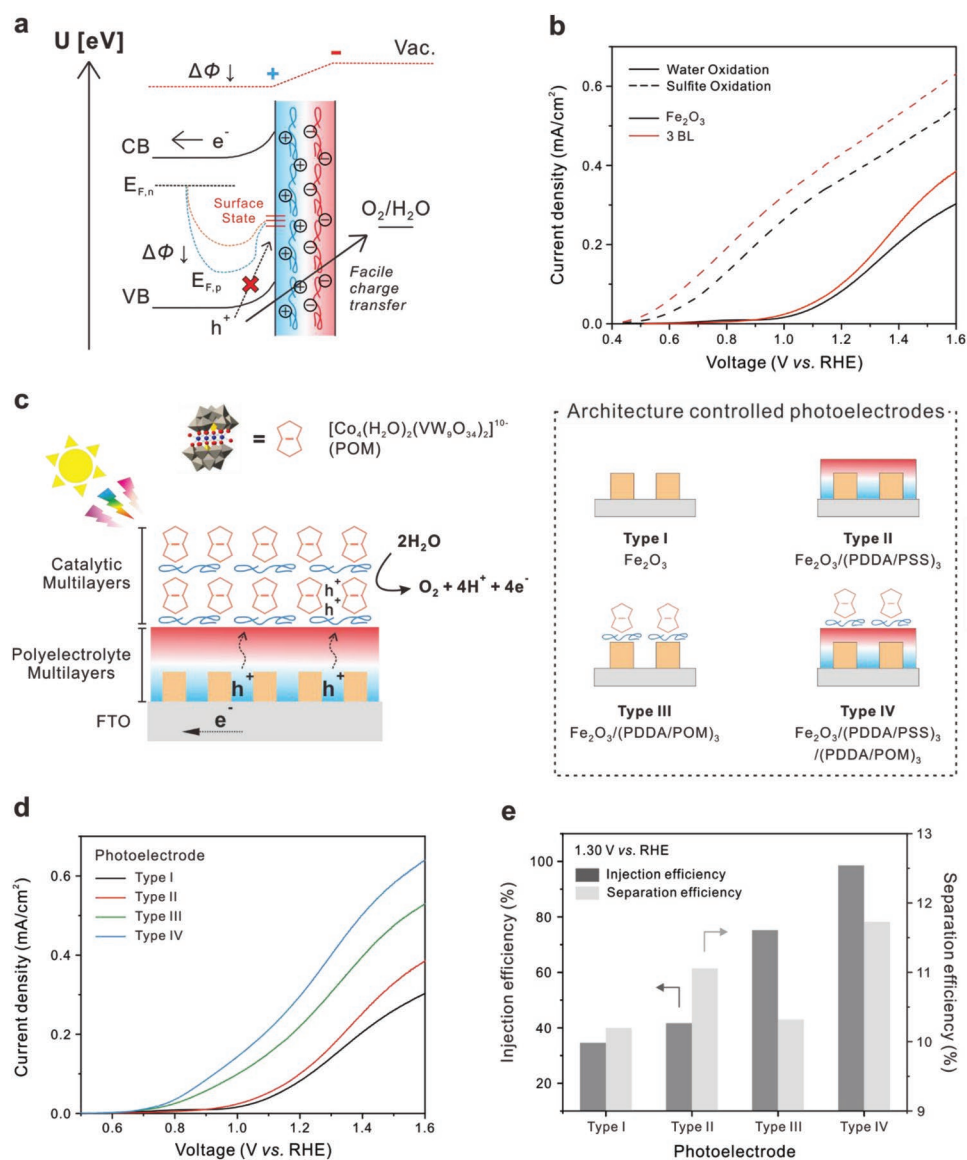


Figure 4. a) Schematic representation showing the improved charge separation efficiency of photoanode after deposition of polyelectrolyte multilayers. b) LSV curves demonstrating the enhanced PEC water oxidation of polyelectrolyte multilayers on Fe_2O_3 with and without sacrificial electron donor (1.0 M Na_2SO_3). c) Schematic representations of photoanodes with additional catalytic multilayer assembled atop different architectures of photoanodes (Types I-IV). d) LSV curves and e) the charge injection and charge separation efficiencies of the corresponding photoelectrodes.

modified with a water oxidation catalyst in a format of catalytic multilayer using the LbL assembly. As a representative example, anionic Co-based polyoxometalate (POM) was deposited on Fe_2O_3 using cationic PDDA as an electrostatic counterpart, e.g., $Fe_2O_3/(PDDA/PSS)_3/(PDDA/POM)_3$ (type IV). For comparison, we prepared three control sets: Fe_2O_3 (type I), $Fe_2O_3/(PDDA/PSS)_3$ (type II), and $Fe_2O_3/(PDDA/POM)_3$ (type III) (Figure 4c). As shown in Figure 4d, the co-deposition of the polyelectrolyte dipole and catalytic multilayers led to the highest performance due to the improved charge separation and injection efficiencies by the polyelectrolyte multilayers and POM catalysts, respectively. While the charge separation efficiency was improved significantly in the presence of the interfacial dipole layers, the charge injection efficiency was improved considerably in the

presence of POM catalysts (Figure 4e). These results indicate that our approach can be combined with other approaches or functional materials for developing highly efficient photoelectrodes, which again highlights the unique opportunities of modular LbL assembly in functional nanoelectrodes.

Finally, the substrate- and pH-independent universal application of our LbL approach was demonstrated using TiO_2 nanotubes (NTs) as a photoanode. Anodized TiO_2 NTs were prepared and modified with polyelectrolyte multilayers composed of cationic PDDA and anionic PSS using the identical LbL assembly. According to TEM and EDS analyses (Figure 5a-c), bright and thin polyelectrolyte multilayers composed of S and N from PSS and PDDA, respectively, were uniformly and conformally coated on the surface of TiO_2 NTs. In accordance with the

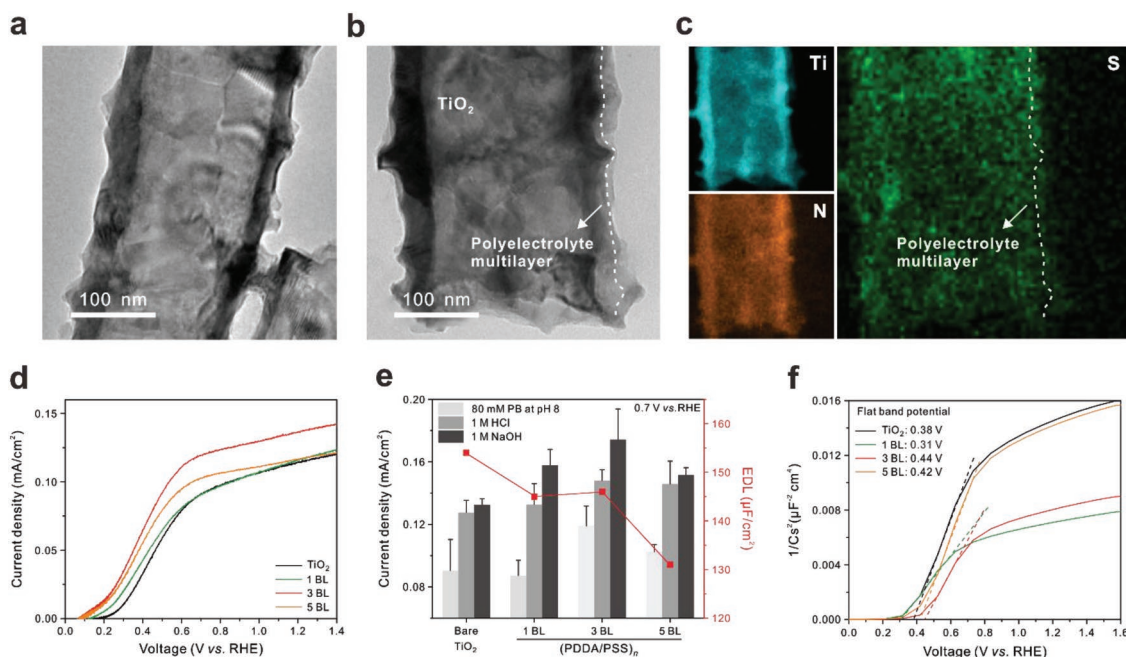


Figure 5. TEM images of a) bare TiO₂ NTs and b) TiO₂ NTs modified with polyelectrolyte multilayers. c) EDS mapping images of TiO₂ NTs after deposition of polyelectrolyte multilayers. d) LSV curves of bare TiO₂ NTs and TiO₂ NTs assembled with polyelectrolyte multilayers (1, 3, and 5 BL). e) Comparison of PEC performance with electric double layer capacitance as a function of number of BLs under various electrolyte conditions, and f) Mott–Schottky plot of bare TiO₂ NTs and TiO₂ NTs assembled with polyelectrolyte multilayers.

result observed for the Fe₂O₃ photoanodes, TiO₂ NTs exhibited a higher performance when the terminal layer was negatively charged PSS (Figure S11a, Supporting Information). Interestingly, the highest performance was obtained when modification was achieved with 3 BL. This coincides with the result of Fe₂O₃ photoanode (Figure 5d and Figure S11b, Supporting Information). Because TiO₂ is highly stable independent of external pHs, we examined the effect of the polyelectrolyte-based dipole layers on efficient charge separation in a wide pH range from highly acidic (1 M HCl) to basic (1 M NaOH) conditions. Despite the decrease in the surface area (Figure S12, Supporting Information), the charge separation efficiency was improved considerably after the modification with the polyelectrolyte multilayers at all the pH conditions tested due to the formation of interfacial dipole moments (Figure 5e,f).

Compared to conventional approaches, our approach has many advantages in terms of simplicity, general applicability, and compatibility with various strategies for performance improvements (Table S1, Supporting Information). In this study, we demonstrated that the charge separation efficiency of photoanodes can be improved by modifying their surface with polyelectrolyte-assembled interfacial dipole layers. In principle, rather than polyelectrolytes, one can utilize ferroelectric oxide as a photoelectrode or as a dipole layer for efficient separation of photogenerated charge carriers.^[48] However, most ferroelectric oxides (e.g., BaTiO₃ and SrTiO₃) are wide bandgap semiconductors and thus, exhibit low utility; they cannot harvest visible light.^[49] Their application as a dipole layer is also limited due to the following issues: i) lattice-matching between the ferroelectric dipole layers and underlying materials is required,^[50,51] ii) a harsh processing condition is required for crystallization

and ferroelectricity,^[52,53] and iii) formation of additional interfaces between them can cause severe recombination.^[54] In contrast, our approach allows a simple modification of various semiconducting photoelectrodes without the introduction of additional interfaces under mild conditions (i.e., aqueous process at ambient temperature and pressure). It can be applied to almost all types of photoelectrodes by taking advantages of versatile LbL assembly. Furthermore, our approach can be readily combined with conventional approaches to improve the performance of photoelectrodes, such as catalyst loading,^[12,20] doping,^[55] defect engineering,^[56] and heterojunction formation.^[28]

3. Conclusion

To summarize, we demonstrated that the charge separation efficiency of water oxidation photoanodes can be modulated by modifying their surface with polyelectrolyte multilayers. Our results indicate that the deposition of cationic and anionic polyelectrolytes induces the formation of interfacial dipoles. The magnitude and direction of the interfacial dipole moments can be controlled precisely by varying the number of BL of oppositely charged polyelectrolytes and the type of the terminal polyelectrolyte in the multilayer. As a result, we can modulate the charge separation efficiency of underlying photoanodes, such as Fe₂O₃ and TiO₂, by precise tuning of the interfacial dipole moments, regardless of the pHs. Further deposition of water oxidation catalysts on top of the polyelectrolyte multilayer-modified photoanodes resulted in significant performance improvement, suggesting the versatility of our approach. We believe that our strategy can be combined with the conventional

approaches for performance improvements, such as catalyst loading, doping, defect engineering, and heterojunction formation, and thereby provide insights for the design and fabrication of efficient photoelectrodes.

4. Experimental Section

Materials: PDDA (M_w 100 000–200 000), PSS ($M_w \approx 70$ 000), $\text{FeCl}_3 \cdot 6\text{H}_2\text{O}$, NH_4F , $\text{Co}(\text{NO}_3)_2 \cdot 6\text{H}_2\text{O}$, $\text{Na}_2\text{WO}_4 \cdot 2\text{H}_2\text{O}$, and NaVO_3 were purchased from Sigma–Aldrich (USA). Ethylene glycol, Ti foil, and NaNO_3 were purchased from Alfa Aesar (USA). All reagents were used without further purification.

Fabrication of Fe_2O_3 Photoanodes: Sn-doped Fe_2O_3 nanowires were grown on fluorine-doped tin oxide (FTO) by the hydrothermal method according to the literature.^[55] Briefly, 0.15 M $\text{FeCl}_3 \cdot 6\text{H}_2\text{O}$ and 1.0 M NaNO_3 were dissolved in deionized (DI) water. Then, HCl was added to adjust the pH to 1.5. The mixed solution (20 mL) was transferred to a Teflon-lined stainless-steel autoclave containing an FTO substrate with its conductive side facing up. β - FeOOH nanowires were formed after hydrothermal reaction at 95 °C for 4 h, sintered in air at 550 °C for 2 h (for conversion to α - Fe_2O_3 nanowires), and annealed at 800 °C for 20 min (for Sn-doping).

Fabrication of TiO_2 Photoanodes: Anodic TiO_2 NTs were synthesized according to the literature.^[57] First, a solution for anodization (30 mL) was prepared by dissolving ethylene glycol (10 wt.%) and NH_4F (0.3 wt.%) in DI water. Anodization was conducted in a two-electrode configuration at 60 V for 30 min using washed Ti foil as the working electrode and Pt as the counter electrode. After anodization, the samples were cleaned with ethanol and DI water and annealed at 450 °C for 2 h at a ramping rate of 2 °C min⁻¹.

Synthesis of $\text{Na}_{10}[\text{Co}_4(\text{H}_2\text{O})_2(\text{VW}_9\text{O}_{34})_2]$ (POM) WOCs: POM water oxidation catalyst was synthesized following procedures in the literature.^[58] 1.2 g of $\text{Co}(\text{NO}_3)_2 \cdot 6\text{H}_2\text{O}$ and 6.0 g of $\text{Na}_2\text{WO}_4 \cdot 2\text{H}_2\text{O}$ were dissolved in 0.50 M sodium acetate buffer (120 mL, pH 4.8) with stirring for 5 min. Then, 0.27 g of NaVO_3 was added to the solution. The mixed solution was refluxed at 80 °C for 2 h. This was followed by hot filtration to remove precipitates and impurities. The filtrate solution was stored in a refrigerator for a week to collect POM crystals by filtration.

Modification of Fe_2O_3 and TiO_2 Photoanodes with Polyelectrolyte Multilayers: Polyelectrolyte multilayers were deposited on photoanodes by the LbL assembly method. Both the cationic and anionic polyelectrolyte solutions for depositing polyelectrolyte multilayers were prepared by dissolving PDDA and PSS, respectively, in DI water at a concentration of 5 mg mL⁻¹ and pH 7. Polyelectrolyte multilayers were deposited on the desired substrate by the following procedure: Each photoanode was dipped into the PDDA and PSS solution for 5 min each. This was followed by washing with DI water for 30 s three times after each immersion step. The above procedures were repeated for the desired number of times.

Characterization: Morphological and surface roughness analysis of photoanodes were carried out using an NX-10 AFM (Park Systems, Korea), a JEM-2100 high-resolution TEM (HR-TEM, JEOL, Japan), and a TECNAI TEM (Thermo Fisher Scientific, USA). The absorbance and thickness of the polyelectrolyte multilayers were measured with a Cary 5000 UV–vis spectrophotometer (Varian, USA) and EC-400/M-2000 V ellipsometer (J. A. Woollam Co. Inc., USA) using quartz and silicon substrates, respectively. Elemental analysis was conducted using an Alpha X-ray photoelectron spectrophotometer (Thermo-Fisher, USA).

PEC Characterization: PEC characterizations were carried out in a three-electrode configuration under front-side illumination. A 300 W Xe lamp was used as a visible and UV/visible light source with and without a 400 nm cut-on filter and an infrared water filter, respectively. For the Fe_2O_3 photoanode, 80 × 10⁻³ M potassium phosphate (pH 8.0) was used as the electrolyte solution. For TiO_2 , 1 M HCl, 80 × 10⁻³ M potassium phosphate (pH 8.0), and 1 M NaOH were used as the electrolyte. To determine the charge separation efficiency, 1 M Na_2SO_4

was additionally introduced as a sacrificial electron donor. A WMPG1000 multichannel potentiostat/galvanostat (WonA Tech Co. Ltd, Korea) was used for regulating the potential of the working electrode under the following conditions: Fe_2O_3 or TiO_2 as the working electrode, Ag/AgCl as the reference electrode, Pt film as the counter electrode, and scan rates of 20 mV s⁻¹ for Fe_2O_3 and 10 mV s⁻¹ for TiO_2 . The active surface area of each electrode was estimated by electrochemical capacitance measurement using cyclic voltammetry (CV) by sweeping the potential in a non-Faradaic region. EIS was carried out under light using a SP-150 (Bio-Logic Science Instruments, France) under the following conditions: applied bias range from 0.4 to 1.6 V versus RHE with a 0.1 V interval, amplitude of 20 mV, and frequency range from 0.1 Hz to 100 kHz. Numerical fitting of EIS data was conducted using EC-Lab software (Bio-Logic Science Instruments, France). Mott–Schottky analysis was carried out using an SP-150 under 20 mV amplitude and 1 kHz frequency. The charging of the surface state ($\Delta V_{\text{charging}}$) was calculated by the following equation:

$$Q_{\text{tot}} = \int C_{\text{SS}} dV \quad (1)$$

$$\Delta V_{\text{charging}} = \frac{Q_{\text{tot}}}{C_{\text{dl}}} \quad (2)$$

where Q_{tot} is the amount of charge stored in the surface state of photoelectrodes, C_{SS} is the surface-state capacitance, and C_{dl} is the EDL capacitance. C_{SS} values as a function of the applied potential V were obtained from electrochemical impedance analysis. The charge carrier injection efficiency (\varnothing_{inj}) and charge-separation efficiency (\varnothing_{sep}) was calculated using the following equation:

$$\varnothing_{\text{inj}} = \frac{J_{\text{H}_2\text{O}}}{J_{\text{scavenger}}} \quad (3)$$

$$\varnothing_{\text{sep}} = \frac{J_{\text{scavenger}}}{J_{\text{max}} \times \varnothing_{\text{abs}}} \quad (4)$$

where $J_{\text{H}_2\text{O}}$ and $J_{\text{scavenger}}$ are the photocurrent densities measured with and without sacrificial electron donor, respectively. J_{max} is the maximum theoretical photocurrent density calculated by the solar photon flux, and \varnothing_{abs} is light-absorption efficiency of Fe_2O_3 according to wavelength.

Supporting Information

Supporting Information is available from the Wiley Online Library or from the author.

Acknowledgements

S.B., D.K., and H.K. contributed equally to this work. This work was supported by the National Research Foundation of Korea (NRF-2017R1A2B3012148 and NRF-2018R1D1A1A02046918). It was also supported by the Nano-Material Technology Development Program (2017M3A7B4052802) through the National Research Foundation of Korea (NRF) funded by the Ministry of Science and ICT of Korea.

Conflict of Interest

The authors declare no conflict of interest.

Keywords

charge separation, interfacial dipole, layer-by-layer assembly, photoelectrodes, polyelectrolyte multilayers

Received: October 15, 2019

Revised: November 18, 2019

Published online:

- [1] Y. Tachibana, L. Vayssieres, J. R. Durrant, *Nat. Photonics* **2012**, *6*, 511.
- [2] K. Sivula, R. van de Krol, *Nat. Rev. Mater.* **2016**, *1*, 15010.
- [3] S. Bae, J. E. Jang, H. W. Lee, J. Ryu, *Eur. J. Inorg. Chem.* **2019**, *2019*, 2040.
- [4] W. Tu, Y. Zhou, Z. Zou, *Adv. Mater.* **2014**, *26*, 4607.
- [5] K. Maeda, T. E. Mallouk, *Bull. Chem. Soc. Jpn.* **2019**, *92*, 38.
- [6] N. Roy, N. Suzuki, C. Terashima, A. Fujishima, *Bull. Chem. Soc. Jpn.* **2019**, *92*, 178.
- [7] G. M. Carroll, D. K. Zhong, D. R. Gamelin, *Energy Environ. Sci.* **2015**, *8*, 577.
- [8] J. Y. Kim, J. W. Jang, D. H. Youn, G. Magesh, J. S. Lee, *Adv. Energy Mater.* **2014**, *4*, 1400476.
- [9] Y. Choi, D. Jeon, Y. Choi, D. Kim, N. Kim, M. Gu, S. Bae, T. Lee, H. W. Lee, B. S. Kim, J. Ryu, *ACS Nano* **2019**, *13*, 467.
- [10] T. W. Kim, K.-S. Choi, *Science* **2014**, *343*, 990.
- [11] Y. M. Ma, A. Kafzas, S. R. Pendlebury, F. Le Formal, J. R. Durrant, *Adv. Funct. Mater.* **2016**, *26*, 4951.
- [12] S. Bae, H. Kim, D. Jeon, J. Ryu, *ACS Appl. Mater. Interfaces* **2019**, *11*, 7990.
- [13] J. H. Baek, B. J. Kim, G. S. Han, S. W. Hwang, D. R. Kim, I. S. Cho, H. S. Jung, *ACS Appl. Mater. Interfaces* **2017**, *9*, 1479.
- [14] J. J. Zhang, X. X. Chang, C. C. Li, A. Li, S. S. Liu, T. Wang, J. L. Gong, *J. Mater. Chem. A* **2018**, *6*, 3350.
- [15] D. Jeon, N. Kim, S. Bae, Y. Han, J. Ryu, *ACS Appl. Mater. Interfaces* **2018**, *10*, 8036.
- [16] S. Kment, F. Riboni, S. Pausova, L. Wang, L. Wang, H. Han, Z. Hubicka, J. Krysa, P. Schmuki, R. Zboril, *Chem. Soc. Rev.* **2017**, *46*, 3716.
- [17] Z. P. Zeng, T. Li, Y. B. Li, X. C. Dai, M. H. Huang, Y. H. He, G. C. Xiao, F. X. Xiao, *J. Mater. Chem. A* **2018**, *6*, 24686.
- [18] S. W. Boettcher, E. L. Warren, M. C. Putnam, E. A. Santori, D. Turner-Evans, M. D. Kelzenberg, M. G. Walter, J. R. McKone, B. S. Brunschwig, H. A. Atwater, N. S. Lewis, *J. Am. Chem. Soc.* **2011**, *133*, 1216.
- [19] R. L. Fan, W. Dong, L. Fang, F. G. Zheng, M. R. Shen, *J. Mater. Chem. A* **2017**, *5*, 18744.
- [20] L. F. Pan, J. H. Kim, M. T. Mayer, M. K. Son, A. Ummadisingu, J. S. Lee, A. Hagfeldt, J. S. Luo, M. Gratzel, *Nat. Catal.* **2018**, *1*, 412.
- [21] A. Paracchino, V. Laporte, K. Sivula, M. Gratzel, E. Thimsen, *Nat. Mater.* **2011**, *10*, 456.
- [22] M. R. Nellist, J. J. Qiu, F. A. L. Laskowski, F. M. Toma, S. W. Boettcher, *ACS Energy Lett.* **2018**, *3*, 2286.
- [23] Y. Kageshima, T. Fujita, F. Takagi, T. Minegishi, K. Teshima, K. Domen, Y. Amano, H. Nishikiori, *ChemElectroChem* **2019**, *6*, 4859.
- [24] E. Kemppainen, A. Bodin, B. Sebok, T. Pedersen, B. Seger, B. Mei, D. Bae, P. C. K. Vesborg, J. Halme, O. Hansen, P. D. Lund, I. Chorkendorff, *Energy Environ. Sci.* **2015**, *8*, 2991.
- [25] M. Kan, D. Q. Xue, A. H. Jia, X. F. Qian, D. T. Yue, J. P. Jia, Y. X. Zhao, *Appl. Catal., B* **2018**, *225*, 504.
- [26] C. Zachaus, F. F. Abdi, L. M. Peter, R. van de Krol, *Chem. Sci.* **2017**, *8*, 3712.
- [27] F. Lin, S. W. Boettcher, *Nat. Mater.* **2014**, *13*, 81.
- [28] S. Y. Chae, C. S. Lee, H. Jung, O. S. Joo, B. K. Min, J. H. Kim, Y. J. Hwang, *ACS Appl. Mater. Interfaces* **2017**, *9*, 19780.
- [29] S. H. Shen, S. A. Lindley, X. Y. Chen, J. Z. Zhang, *Energy Environ. Sci.* **2016**, *9*, 2744.
- [30] W. Zhang, R. Chen, Z. Yin, X. Wang, Z. Wang, F. Fan, Y. Ma, *ACS Appl. Mater. Interfaces* **2019**, *11*, 34000.
- [31] J. Zheng, Y. Lyu, R. Wang, C. Xie, H. Zhou, S. P. Jiang, S. Wang, *Nat. Commun.* **2018**, *9*, 3572.
- [32] W. Cui, Z. Xia, S. Wu, F. Chen, Y. Li, B. Sun, *ACS Appl. Mater. Interfaces* **2015**, *7*, 25601.
- [33] J. Y. Zheng, H. J. Zhou, Y. Q. Zou, R. L. Wang, Y. H. Lyu, S. P. Jiang, S. Y. Wang, *Energy Environ. Sci.* **2019**, *12*, 2345.
- [34] J. Li, S. K. Cushing, P. Zheng, F. Meng, D. Chu, N. Wu, *Nat. Commun.* **2013**, *4*, 2651.
- [35] J. Yu, A. Kudo, *Adv. Funct. Mater.* **2006**, *16*, 2163.
- [36] Y. C. Zhang, N. Afzal, L. Pan, X. Zhang, J. J. Zou, *Adv. Sci.* **2019**, *6*, 1900053.
- [37] D. Kim, M. Gu, M. Park, T. Kim, B. S. Kim, *Mol. Syst. Des. Eng.* **2019**, *4*, 65.
- [38] H. Kim, Y. You, D. Kang, D. Jeon, S. Bae, Y. Shin, J. Lee, J. Lee, J. Ryu, *Adv. Funct. Mater.* <https://doi.org/10.1002/adfm.201906407>.
- [39] G. Ladam, P. Schaad, J. C. Voegel, P. Schaaf, G. Decher, F. Cuisinier, *Langmuir* **2000**, *16*, 1249.
- [40] N. Torasso, J. M. Armaleo, M. Tagliacucchi, F. J. Williams, *Langmuir* **2017**, *33*, 2169.
- [41] S. Yang, D. Prendergast, J. B. Neaton, *Nano Lett.* **2012**, *12*, 383.
- [42] J. G. Chen, C. W. Jones, S. Linic, V. R. Stamenkovic, *ACS Catal.* **2017**, *7*, 6392.
- [43] C. C. McCrory, S. Jung, J. C. Peters, T. F. Jaramillo, *J. Am. Chem. Soc.* **2013**, *135*, 16977.
- [44] B. Klahr, S. Gimenez, F. Fabregat-Santiago, J. Bisquert, T. W. Hamann, *J. Am. Chem. Soc.* **2012**, *134*, 16693.
- [45] B. Klahr, S. Gimenez, F. Fabregat-Santiago, T. Hamann, J. Bisquert, *J. Am. Chem. Soc.* **2012**, *134*, 4294.
- [46] O. Zandi, T. W. Hamann, *Nat. Chem.* **2016**, *8*, 778.
- [47] J. Schneider, D. W. Bahnemann, *J. Phys. Chem. Lett.* **2013**, *4*, 3479.
- [48] F. Chen, H. Huang, L. Guo, Y. Zhang, T. Ma, *Angew. Chem., Int. Ed.* **2019**, *58*, 10061.
- [49] S. Das, S. Ghara, P. Mahadevan, A. Sundaresan, J. Gopalakrishnan, D. D. Sarma, *ACS Energy Lett.* **2018**, *3*, 1176.
- [50] P. Zhou, A. V. Singh, Z. Li, M. A. Popov, Y. Liu, D. A. Filippov, T. Zhang, W. Zhang, P. J. Shah, B. M. Howe, M. E. McConney, G. Srinivasan, M. R. Page, A. Gupta, *Phys. Rev. Appl.* **2019**, *11*, 054045.
- [51] J. Lyu, I. Fina, R. Solanas, J. Fontcuberta, F. Sanchez, *Sci. Rep.* **2018**, *8*, 495.
- [52] W. Ji, K. Yao, Y.-F. Lim, Y. C. Liang, A. Suwardi, *Appl. Phys. Lett.* **2013**, *103*, 062901.
- [53] Z.-M. Wang, K. Zhao, X.-L. Guo, W. Sun, H.-L. Jiang, X.-Q. Han, X.-T. Tao, Z.-X. Cheng, H.-Y. Zhao, H. Kimura, G.-L. Yuan, J. Yin, Z.-G. Liu, *J. Mater. Chem. C* **2013**, *1*, 522.
- [54] E. Jia, D. Wei, P. Cui, J. Ji, H. Huang, H. Jiang, S. Dou, M. Li, C. Zhou, W. Wang, *Adv. Sci.* **2019**, *6*, 1900252.
- [55] Y. Ling, G. Wang, D. A. Wheeler, J. Z. Zhang, Y. Li, *Nano Lett.* **2011**, *11*, 2119.
- [56] J. Nowotny, M. A. Alim, T. Bak, M. A. Idris, M. Ionescu, K. Prince, M. Z. Sahdan, K. Sopian, M. A. Mat Teridi, W. Sigmund, *Chem. Soc. Rev.* **2015**, *44*, 8424.
- [57] Y. R. Smith, B. Sarma, S. K. Mohanty, M. Misra, *ACS Appl. Mater. Interfaces* **2012**, *4*, 5883.
- [58] Q. Yin, J. M. Tan, C. Besson, Y. V. Geletii, D. G. Musayev, A. E. Kuznetsov, Z. Luo, K. I. Hardcastle, C. L. Hill, *Science* **2010**, *328*, 342.